BULLETIN OF THE POLISH ACADEMY OF SCIENCES
TECHNICAL SCIENCES, Vol. 74(3), 2026, Article number: e158299
DOI: 10.24425/bpasts.2026.158299

Detection of vehicle mass using dynamic response to sinusoidal steering excitation

Tomasz PUSTY*, **Marcin MIETEŃ**, and **Włodzimierz KUPICZ**

The Military Institute of Armoured and Automotive Technology, 05-070 Sulejówek k. Warszawy, Poland

Abstract. This study proposes a method for estimating vehicle load using sinusoidal steering excitation and analysis of dynamic responses: lateral velocity (LV), roll velocity (RV) and yaw velocity (YV). The approach enables reliable discrimination between unloaded (W1) and loaded (W2) vehicle states under real driving conditions. Lateral velocity increases with vehicle speed and exhibits higher magnitudes for the loaded state, particularly within the 0.5–1.5 Hz range. Phase responses for W2 show stronger negative shifts and earlier transitions, indicating increased dynamic delay, which makes LV a useful supplementary indicator, especially at medium speeds. Roll velocity (RV) is identified as the most sensitive and repeatable response, and serves as the primary diagnostic variable. The largest differences between loading states occur within the 0.9–1.3 Hz range, where W2 responses exhibit higher amplitudes and a shift toward lower frequencies, directly reflecting increased vehicle mass. Above 2 Hz, system damping increases and load-related differences diminish. Yaw velocity (YV) shows amplitudes 1–3 dB higher for W2 within the 0.6–1.6 Hz range, together with phase shifts, but its sensitivity is lower than that of RV, classifying it as a supplementary indicator. Unlike methods based on complex identification algorithms or high-frequency measurements, this study adopts a simplified linear single-degree-of-freedom (1-DoF) oscillator model. Defined road-test conditions, including speeds of 45–56 km/h and excitation near 1.0 Hz, ensure dominance of a single dynamic mode. The method is computationally efficient and cost-effective, although its linear formulation may limit accuracy under strongly nonlinear dynamics or varying road conditions.

Keywords: vehicle mass estimation; sinusoidal steering wheel excitation; dynamic response differentiation.

1. INTRODUCTION

In the literature, increasing emphasis is placed on the growing importance of autonomous and unmanned vehicles in reconnaissance and logistics tasks, with obstacle-detection sensors being critical for their effectiveness, as they enable adaptation of the vehicle to variable operational conditions [1]. Experimental research on UGVs is still in its early stages, lacking standardized scenarios and guidelines for evaluating vehicle dynamic response under varying loads and speeds [2]. Experiments with vehicles moving in convoys have demonstrated that convoy speed depends on the vehicle type (wheeled or tracked) and on interaction with a human-driven vehicle. On-board devices recording motion parameters following an accident, such as ADR (accident data recorder), make it possible to reconstruct the exact trajectory of motion, but only retrospectively [3]. However, planning of the trajectory to be followed by a vehicle requires an appropriately selected dynamic model of motion that accounts for the current state of the vehicle, including its load condition.

The continuous growth in the number of sensors, recorders, and actuators in vehicles, their technical advancement, intersystem information exchange, and the processing of large amounts of measurement data in near-real time facilitate improved predictive modeling. These developments, in turn, support the design of new driver-assistance systems, such as automatic lane-change functionalities. The more accurate the model and the more precise the input data for computations, the more effectively the vehicle's trajectory can be planned. Predictive models rely on real-time sensor data. Of particular significance are signals from sensors measuring longitudinal and lateral accelerations as well as angular velocities of a selected vehicle point [4, 5], alongside current vehicle parameters.

The literature devotes considerable attention to simple models due to their computational efficiency, but increasingly also to more complex vehicle dynamics models, given the ever-growing computational capabilities. Simplified so-called "bicycle models" enable sensitivity analysis of a vehicle's lateral dynamics as a function of vehicle parameters and control strategies. This, in turn, allows for evaluation of the influence of speed and payload on the vehicle's response to steering inputs [6]. Analysis of lane-change maneuvers has demonstrated that Kalman controllers combined with simplified reference "bicycle models" enable stable vehicle control even under variable speed and load conditions [7]. Studies of driver maneuvers have shown that errors in resetting acceleration sensor components lead to different deviations of the vehicle's final position [8]. Proper parameterization of control systems is therefore crucial for ensuring safe obstacle avoidance [9]. Simple models of the automobile itself allow for separation of longitudinal, lateral and vertical dynamics as well as for partially analytical derivation of the corresponding equations of motion. These models are usually also approximations used in the design of a state observer and controller intended to influence vehicle behavior [10]. Due to

*e-mail: tomasz.pusty@wp.pl

Manuscript submitted 2026-01-16, revised 2026-01-16, initially accepted for publication 2026-02-22, published in May 2026.

the differing requirements placed on models depending on the type of application, a wide range of driver models is available. An overview of driver models, taking into account their applications as well as various methodological approaches to modeling, is presented in [11].

More detailed models of vehicle dynamics with multiple degrees of freedom are also being developed, but their application requires a broad range of precisely estimated input data [12]. Steering system parameters, suspension characteristics, as well as vehicle load and velocity all affect its dynamic response. Even moderate changes in load, whether by passengers or cargo, significantly influence vehicle dynamics. Additional loading lowers natural vibration frequencies and produces slower, though often more pronounced, dynamic responses. A loaded vehicle is more prone to excessive body roll and delayed steering response [13], and may exhibit shifts in handling characteristics from oversteer to understeer, or vice versa. Therefore, supplying computational models with precise load data is preferable to using broad ranges of potential load variations.

Rapid detection of vehicle load condition can be achieved using dedicated suspension deflection sensors, widely employed in trucks, buses and passenger cars with height-adjustable suspensions. However, challenges arise when attempting to determine the load state of vehicles not equipped with such sensors. In such cases, a short test involving dynamic steering-wheel excitation may be employed to estimate load condition [14]. This test consists of a road experiment in which the steering wheel is subjected to sinusoidal excitation. During the test, selected physical quantities describing both the input and the vehicle's response are recorded. Sinusoidal steering-wheel excitation is a test method in which the steering angle varies according to a sinusoidal function with specified frequency and amplitude. This method is widely used to evaluate vehicle stability at high speeds, handling characteristics (oversteer/understeer), steering system performance and the effectiveness of electronic stability control (ESC).

In [15], it has been shown that vehicle dynamic properties and characteristics can be inferred from responses to steering inputs at excitation frequencies of 0.5 Hz, 1 Hz and 0.75 Hz [16]. Furthermore, [17] demonstrated that sinusoidal frequency sweep allows for full characterization of vehicle response and sensitivity in the frequency domain. In [18], a vehicle mass estimation method based on high-frequency acceleration measurements was proposed, where the longitudinal force information is obtained directly from the electric motor. However, for vehicles with internal combustion engines (ICEs), accurately estimating engine torque remains a significant technical bottleneck. Further progress in this area is expected to enable the adaptation of this estimation method to ICE vehicles. In [19], analysis of yaw velocity and lateral acceleration as functions of steering angle provided valuable insights into nonlinear vehicle dynamic behavior. The work presented in [20] examined increments of transient lateral dynamic response and yaw natural frequencies in the input frequency range of 0–2 Hz, though not for load-state detection. Study [21] attempted to classify vehicles based on ratios of frequency-response amplitudes for sideslip velocity, yaw rate and roll angle. Articles [22, 23] discuss significant model parameter differences, mainly attributable to changes in load, and also introduce an M-type mass estimator (robust against outliers) with a forgetting factor. The vehicle longitudinal dynamics model is being continuously corrected using these parameter estimates, and the vehicle mass is then estimated in real time based on the recursive least squares method with a forgetting factor. Sensitive parameters of the vehicle dynamics model are adaptively adjusted according to changes in the road environment, which effectively improves the accuracy and stability of the road slope and vehicle mass estimation algorithm and ensures its applicability under a wide range of operating conditions. The application of the least squares method, considering the forgetting factor and joint M-estimation in the mass estimation process, can be articulated as described in [24].

The method of sinusoidal steering-wheel excitation is therefore promising as a means of vehicle load detection, though further research is required across different vehicle speeds and a wider range of excitation frequencies. Such an approach would enable precise definition of test conditions, such as speed, steering amplitude and excitation frequency. It is assumed that this method will not require specialized instrumentation; on-board actuators and sensors will suffice. This is feasible in modern vehicles, particularly in those lacking mechanical connections between the steering wheel and steered wheels (steer-by-wire systems). Additionally, ESC system sensors may be utilized for measurement of relevant physical quantities. The steering-wheel angle is among the most critical signals in safety and control systems. The steering angle sensor (SAS) is typically an optical or magnetic encoder with very high resolution (up to 0.1°), integrated within the column integration module (CIM). In modern EPS (electric power steering) systems, SAS constitutes an integral component. These sensors usually operate at 100–200 Hz, with CAN bus packet transmission at 50–100 Hz, which is sufficient for ESC and ADAS systems.

As for lateral velocity measurement, dedicated sensors are generally not available in production vehicles, but this parameter can be derived from yaw rate, wheel speeds, lateral acceleration and steering angle. Such computations are performed at 50–100 Hz by ESC or IMU (inertial measurement unit). Yaw velocity (rotation about the vertical axis) and roll velocity (rotation about the longitudinal axis) are typically obtained from gyroscopes integrated within IMU, with sampling frequencies of 50–200 Hz. These data can be accessed via the controller area network (CAN).

Based on these considerations, the objective of this study is to analyze the feasibility of detecting vehicle load condition using recorded signals of sinusoidal steering-wheel excitation and corresponding responses, namely lateral velocity, yaw velocity and roll velocity. This study focuses on experimental analysis of the vehicle's dynamic response and of the linear second-order oscillator (1-DoF) in roll in the context of mass detection. The experiments encompass a broad range of steering excitations, with the ultimate goal of narrowing them to a selected excitation frequency and a single sinusoidal period, which might occur during a lane-change maneuver.

2. EXPERIMENTAL PROCEDURE

2.1. Test object and conditions

The test object was a Jeep Wrangler off-road vehicle, shown in Fig. 1. The experiments were conducted on a closed section of the airfield in Biała Podlaska, Poland. The airfield surface was dry, clean and flat, with a high tire-road adhesion coefficient ($\mu = 0.8–0.9$). Average wind speed did not exceed 2 m/s in gusts. Tests were carried out at constant vehicle speeds along a designated test track with a dry and homogeneous surface. A moderate steering-wheel excitation amplitude was adopted to remain within the range of small sideslip angles. The input to the linear system was a sinusoidal signal with amplitude $A = 63°$ and a linearly increasing frequency within the range of 0.5–2.5 Hz. The excitation amplitude is important; however, in the proposed method, its role is secondary to that of the excitation frequency. The 63° amplitude refers to the steering-wheel angle. With a steering ratio of approximately 18:1, this corresponds to a front-wheel steering angle of about 3.5°. The amplitude should be sufficiently small to ensure that the system operates in a quasi-linear range and to avoid nonlinearities resulting from suspension component saturation or the activation of stability control systems. With a constant excitation amplitude, the applied frequency response function analysis normalizes the vehicle response with respect to the input signal, so that load state identification is based primarily on changes in the dynamic characteristics rather than on the absolute signal levels. No mechanical parameters were changed. The apparent stiffness change results from the increased mass.

Fig. 1. View of the test object

The vehicle was driven at target test speeds of 21 km/h, 35 km/h, 45 km/h, 55 km/h and 65 km/h. Three test runs were performed at each speed, and the results from one representative run were selected for analysis.

The tests were conducted for the following vehicle load variants: vehicle curb weight plus the mass of the driver, the measurement operator and the steering robot – W1; additional load placed on the cargo compartment floor – W2.

The results of the mass measurements are presented in Table 1, while the results of the center of gravity (CG) position measurements are shown in Table 2.

Table 1
Results of mass measurements

Measured parameter	Mass W1 [kg]	Mass W2 [kg]
Mass on the front axle	1330	1290
Mass on the rear axle	1410	1670
Vehicle weight	2740	2960

Table 2
Position of the center of gravity

Distance of the center of gravity from	Variant	
	W1	W2
the front axle of the vehicle	1518 mm	1664 mm
the road surface	742 mm	711 mm
the vehicle's longitudinal plane of symmetry	9 mm	6 mm

2.2. Measurement equipment and adopted reference frames

The measurement system employed in the study consisted of an OXTS RT 3000 v3 inertial-satellite unit, an AB Dynamics SR60 steering robot, a data acquisition card, steering angle and torque sensors, power supply batteries, and data recording computers. The signal recording frequency was 100 Hz. The power supply block and the robot's central unit, OXTS RT 3000 v3, as well as the robot actuator block, are shown in Fig. 2 and 3.

Fig. 2. View of the power supply block (silver) and robot central unit (blue), OXTS RT 3000 v3 (red)

A local coordinate system rigidly attached to the vehicle body was adopted. The x-axis was oriented forward in the vehicle's longitudinal plane of symmetry; the y-axis was perpendicular to this plane and oriented to the driver's left; and the z-axis

Fig. 3. View of the robot actuator block

was directed upward. The following quantities were measured during the experiments: three mutually orthogonal components of the linear acceleration vector (with use of a triaxial OXTS RT 3000 v3 inertial-satellite unit accelerometer) and angular velocity (with use of a triaxial OXTS RT 3000 v3 inertial-satellite unit gyroscope), rigidly mounted to the vehicle body close to the CG about three perpendicular axes; components of linear velocity along perpendicular axes, i.e. longitudinal and lateral (obtained by IMU-sensor fusion); steering-wheel angle and steering torque.

3. MEASUREMENT RESULTS

The measurement results are presented in the form of signal time histories: steering-wheel angle – Kk(t), lateral velocity – LV(t), yaw velocity – YV(t), and roll velocity – RV(t). Despite considerable effort involved and numerous trials (30 runs with data acquisition in this analysis), vehicle speed stability during testing was maintained within ±1 km/h, which was deemed fully satisfactory. Consequently, slight deviations in vehicle speed can be observed in the plots presented below (Fig. 4). The complete dataset comprises vehicle response signals to sinusoidal steering-wheel angle excitation (Kk) at various vehicle speeds (21, 35(34), 45(44), 56, and 64(63) km/h) and under two load conditions: W1 – unloaded vehicle, W2 – loaded vehicle. High coherence confirms that the body response is driven by the steering input applied. The plots analyze the following responses: LV – lateral velocity, RV – roll velocity and YV – yaw velocity.

The time-domain analysis was carried out using three measured signals: lateral velocity (LV), roll velocity (RV) and yaw velocity (YV). For each driving speed (21, 35, 45, 56 and 64 km/h), the dynamic response was quantified using two metrics: signal amplitude and root-mean-square (RMS) value. RMS values were calculated after removing the mean component, thus representing the energy of the oscillatory response only.

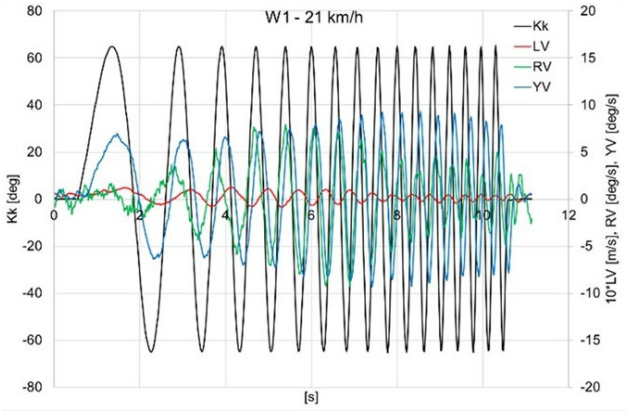

(a)

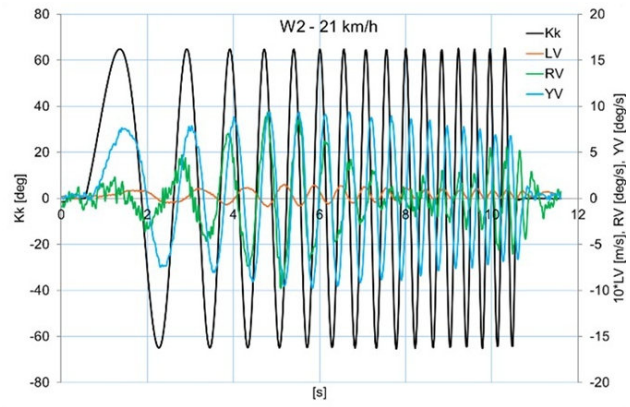

(b)

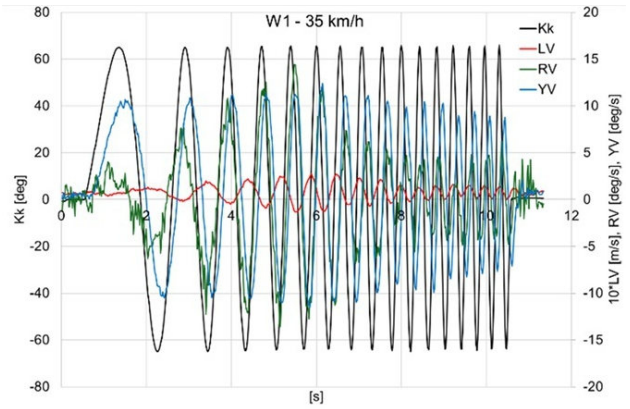

(c)

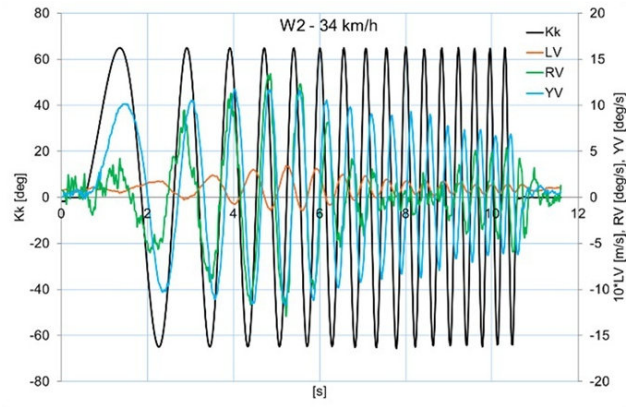

(d)

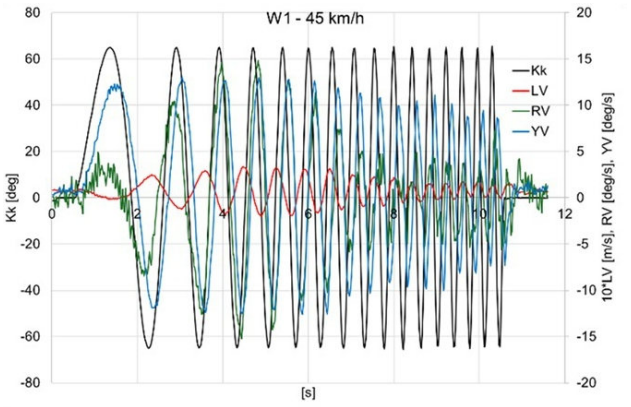

(e)

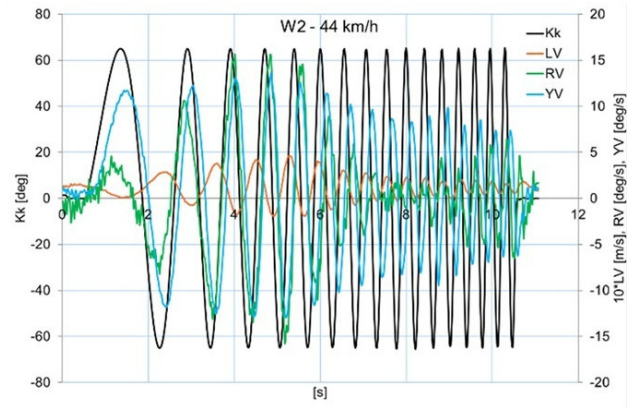

(f)

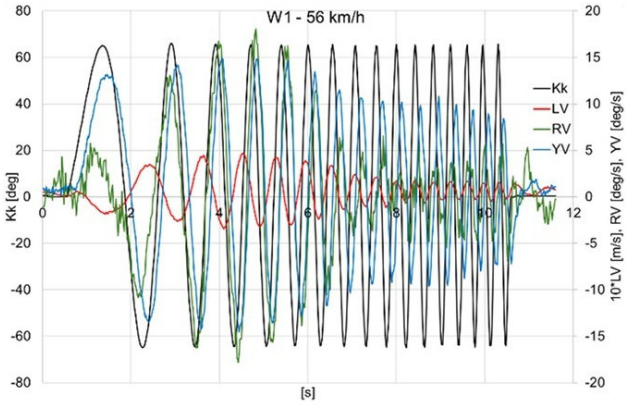

(g)

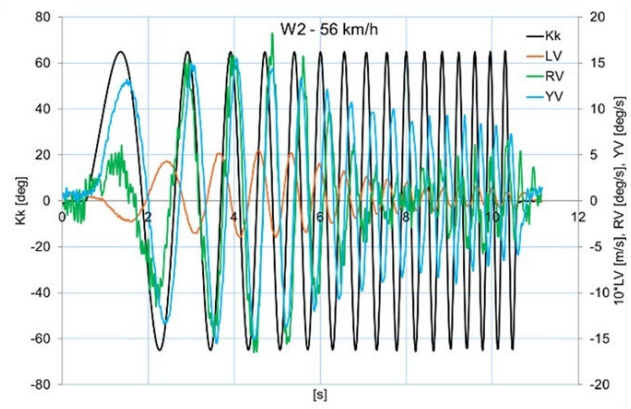

(h)

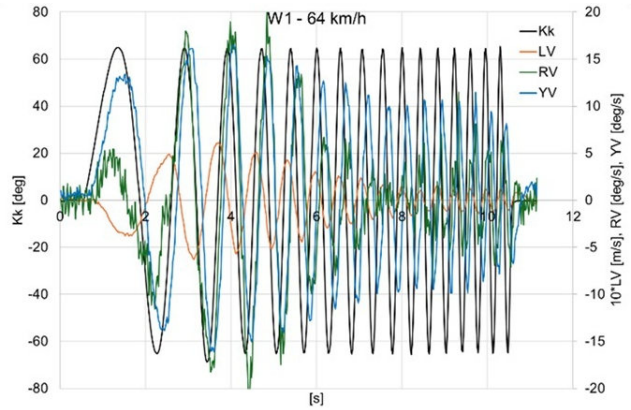

(i)

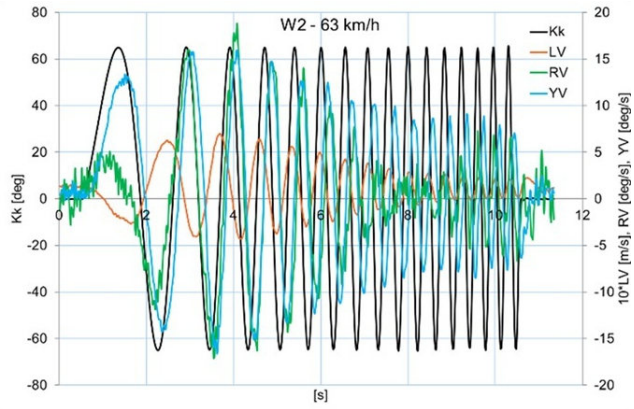

(j)

Fig. 4. Measurement results of steering input Kk and responses: LV, YV, and RV

The measurable indicators (for x = LV, RV and YV), computed over the same time window, are:

(a) the steady-state amplitude:

$$A_{\xi} = \frac{1}{2}\big(\max(x) - \min(x)\big); \tag{1}$$

(b) root-mean-square (RMS) of the response:

$$\mathrm{RMS}_x = \sqrt{\frac{1}{T}\int_0^T x(t)^2\,\mathrm{d}t}\,. \tag{2}$$

Results of time domain calculations are shown in Tables 3 and 4. Analysis was performed over the same time interval (e.g. from the moment excitation enters the 0.9–1.3 Hz band until it leaves it), since the comparison refers to identical excitation conditions.

The results show a clear monotonic increase of both amplitude and RMS with vehicle speed for all analyzed signals. For example, the $\mathrm{RMS}_{\mathrm{LV}}$ increases approximately fivefold between 21 and 64 km/h. At the same time, RV and YV also exhibit pronounced growth, confirming that the vehicle enters a progressively more dynamic operating regime at higher speeds. The sensitivity of

Table 3
Time domain calculation results for W1

Speed [km/h]	A_{LV} [m/s]	RMS_{LV} [m/s]	A_{RV} [deg/s]	RMS_{RV} [deg/s]	A_{YV} [deg/s]	RMS_{YV} [deg/s]
21	0.1	0.05	8.6	3.37	9.3	5.14
35	0.2	0.08	14.0	5.15	11.9	6.76
45	0.3	0.12	15.0	5.82	12.7	7.31
56	0.4	0.17	18.0	6.74	14.6	7.78
64	0.6	0.25	21.1	7.26	16.1	8.39

Table 4
Time domain calculation results for W2

Speed [km/h]	A_{LV} [m/s]	RMS_{LV} [m/s]	A_{RV} [deg/s]	RMS_{RV} [deg/s]	A_{YV} [deg/s]	RMS_{YV} [deg/s]
21	0.1	0.05	9.5	3.19	9.5	5.42
34	0.2	0.09	13.1	4.71	11.6	6.32
44	0.3	0.13	15.7	5.75	13.1	7.07
56	0.5	0.21	17.4	6.52	15.3	7.72
63	0.6	0.25	18.0	6.69	15.9	7.89

the three signals to the vehicle dynamics differs significantly. LV and YV show a stronger growth of amplitude and RMS with speed than RV, which means that lateral and yaw motions are more directly amplified by the increasing excitation energy. In contrast, RV shows a more moderate growth of time-domain amplitudes, but retains a stable oscillatory structure over the entire speed range. This makes RV particularly suitable for further frequency-domain analysis, where its resonance behavior can be robustly identified. From the perspective of vehicle mass and load diagnostics, this means that RV constitutes the most reliable diagnostic channel. While LV and YV show larger absolute amplitudes, they are more sensitive to nonlinearities and test conditions and therefore mainly serve as auxiliary signals for test validation and quality assessment. Finally, the increase of RMS and amplitude above approximately 45 km/h indicates that this speed range provides sufficiently strong excitation of the vehicle dynamics, making it particularly suitable for diagnostic tests aimed at detecting changes in vehicle mass and suspension characteristics.

For both variants, amplitude and RMS increase with vehicle speed, reflecting increasing dynamic excitation. However, the loaded vehicle (W2) exhibits consistently lower RMS_{LV} and amplitudes than W1, indicating reduced lateral motion susceptibility due to higher inertia. RV shows a strong speed-dependent increase in both variants, but W2 consistently presents lower RMS_{RV} and smoother growth. This indicates a more attenuated roll response in the loaded vehicle, even though no mechanical parameters were modified, which is explained by the downward shift of the roll natural frequency caused by increased mass.

RMS_{YV} and amplitude also increase with speed. However, W2 exhibits lower values across the whole speed range, which corresponds to improved yaw and path stability under load.

Time-domain signals already contain clear information about the vehicle load state, and that RV is the most reliable channel for subsequent frequency-domain-based mass identification.

4. FREQUENCY-DOMAIN ANALYSIS OF MEASUREMENT RESULTS

4.1. Adopted method of processing measurement results

The excitation signal $\mathrm{Kk}(t)$ and the responses $\mathrm{LV}(t)$, $\mathrm{YV}(t)$ and $\mathrm{RV}(t)$ were compared, and the frequency response function was computed using the fast Fourier transform (FFT). The frequency response function presents the output signals in terms of magnitude, phase and coherence. By default, the frequency response function employs 2000 samples and a sampling frequency of 20 kHz, which yields a frequency resolution of 10 Hz. However, FFT adapts to the input signals, and there is no limitation on FFT size. A Hanning window was applied to reduce spectral leakage by tapering the signal to zero at the edges of the sampled segment, thereby avoiding discontinuities in FFT. The spectra were rescaled to single-sided magnitude and phase spectra (only the positive FFT frequencies were retained, and their amplitudes were multiplied by a factor of 2 to preserve the signal amplitude). For input of the linear system, a sinusoidal signal was assumed:

$$\mathrm{Kk}(t) = A\sin(\omega t) \tag{3}$$

while at the output, in steady state, the sinusoidal signal had an amplitude of:

$$B = A\left|H(\mathrm{j}\omega)\right| \tag{4}$$

and a phase of φ.

In defining the transfer function, it was assumed that the initial conditions were zero, i.e. the system response was solely the result of the excitation. The frequency response was obtained by determining the magnitude of the transfer function for a given frequency ω and the corresponding phase angle $\varphi(\omega)$. The magnitude of the transfer function was calculated from the following formula:

$$\left|H(\mathrm{j}\omega)\right| = \frac{A_{\mathrm{WY}}}{A_{\mathrm{WE}}}, \tag{5}$$

where: $H(\mathrm{j}\omega)$ – magnitude of the frequency response function, i.e. the ratio of the output signal amplitude to the input signal amplitude; A_{WY} – amplitude spectrum of the output signal, LV, YV and RV; A_{WE} – amplitude spectrum of the input signal – Kk.

The phase angle was determined from the following formula:

$$\varphi(\omega) = \varphi_{\mathrm{WE}}(\omega) - \varphi_{\mathrm{WY}}(\omega), \tag{6}$$

where: $\varphi_{\mathrm{WE}}(\omega)$ – phase angle of the input signal; $\varphi_{\mathrm{WY}}(\omega)$ – phase angle of the output signal.

The calculation results are presented in the plots:

a) magnitude response: in linear scale as a function of frequency [Hz];
b) magnitude response: on decibel scale as $20\log_{10}\left|H(\mathrm{j}\omega)\right|$ in [dB] as a function of frequency [Hz];

c) phase response: $\varphi(\omega)$ in [deg] as a function of frequency [Hz].

4.2. Results of frequency-domain analysis

The frequency characteristics (magnitude response in linear and decibel scale, and phase response) of steering input Kk and lateral velocity response LV were obtained for the unloaded and loaded vehicle (W1 and W2) at different driving speeds. The results are presented in Fig. 5, 6 and 7.

In both cases (W1 and W2), increasing speed leads to higher response values (magnitude response) in the lower frequency range (0.5–1.5 Hz). At higher speeds (e.g. 56–64 km/h), the amplitude values are significantly larger, indicating increased system sensitivity to steering excitations – the vehicle responds more quickly to steering-wheel inputs. The characteristics decrease with increasing frequency, which means that the system is more responsive to slow steering motions than to rapid ones. Analysis of LV and YV showed no nonlinearities, confirming no tire slip.

For the loaded vehicle (W2), the response values are higher than in the unloaded state (W1) at comparable speeds. This difference is particularly evident at higher speeds (e.g. 56 and 63 km/h), where the W2 curves reach noticeably higher values than those for W1. Thus, vehicle loading increases the response amplitude, indicating greater lateral susceptibility of the vehicle to steering excitations.

The loaded vehicle (W2) exhibits higher magnitude response values than the unloaded vehicle (W1) at comparable speeds. These differences are particularly pronounced at higher speeds (45–63 km/h), where the W2 curves lie significantly above those of W1. This indicates that loading increases the dynamic susceptibility of the steering system – lateral response is stronger for the same excitation.

Loading mitigates some of the resonant phenomena: in W2, the phase transitions are smoother and more consistent across speeds, whereas in W1 (unloaded), the responses appear more irregular with a greater number of "wraps" (sudden phase jumps) within the 0.3–0.9 Hz range. In W2, the phase transition points (phase jumps) occur at slightly lower frequencies than in W1 – the added mass shifts the dynamics "to the left" (toward lower frequencies).

For frequencies $f \geq 1$ Hz, the loaded vehicle generally exhibits a negative phase (greater delay) for the same speeds, which indicates that the lateral velocity response lags further behind

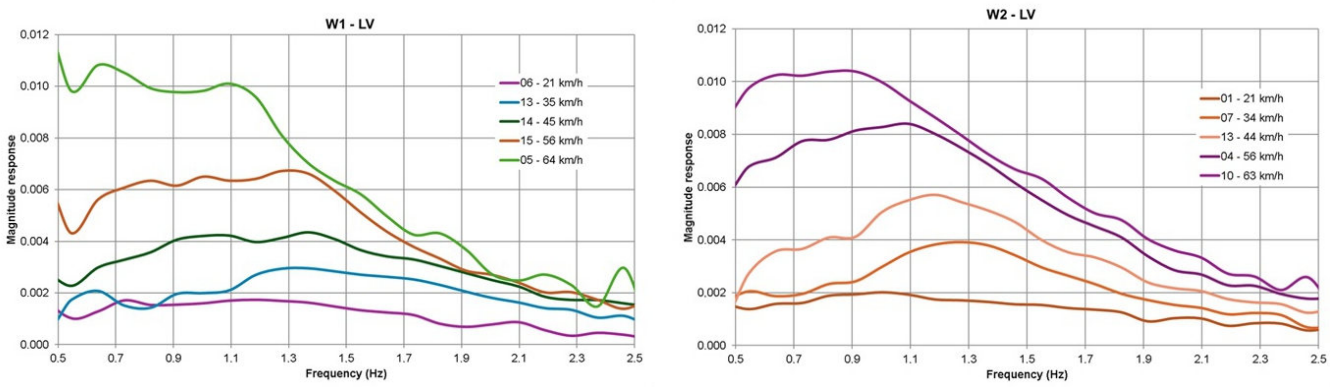

(a) (b)

Fig. 5. Frequency response characteristics (magnitude response) of steering input Kk and lateral velocity response LV for the vehicle: (a) unloaded – W1, (b) loaded – W2

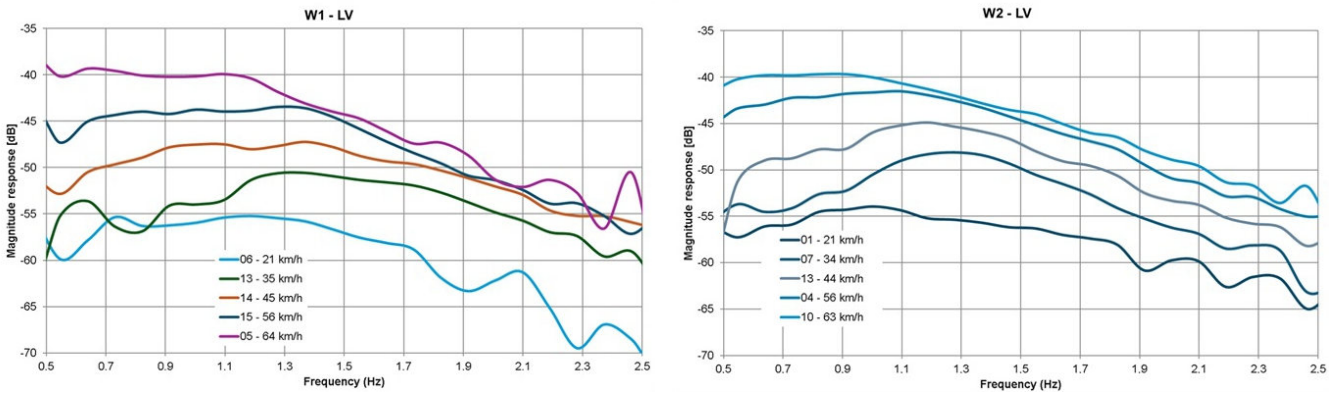

(a) (b)

Fig. 6. Frequency response characteristics (magnitude response on decibel scale) of steering input Kk and lateral velocity response LV for the vehicle: (a) unloaded – W1, (b) loaded – W2

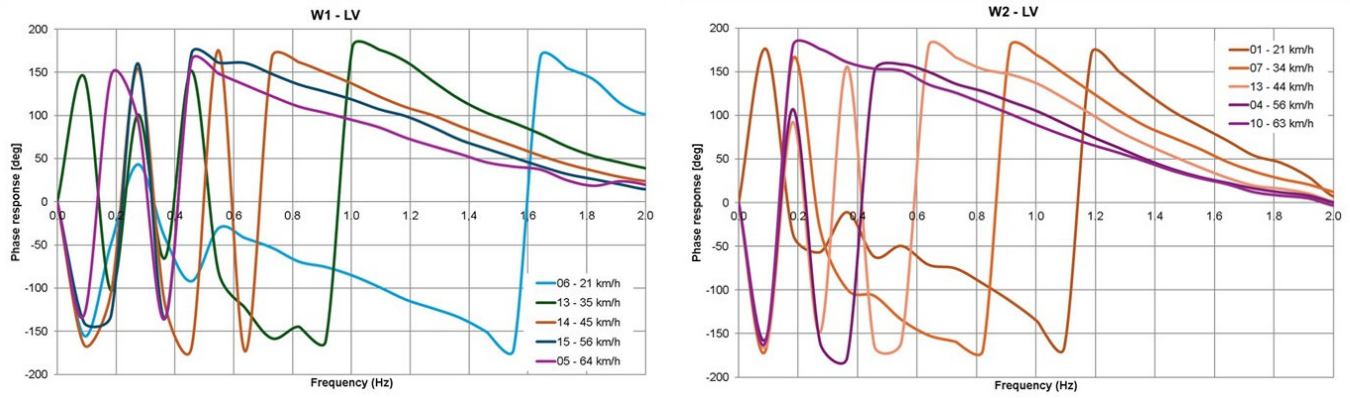

(a) (b)

Fig. 7. Frequency response characteristics (phase response) of steering input Kk and lateral velocity response LV for the vehicle: (a) unloaded – W1, (b) loaded – W2

fast steering inputs. With increased loading, the phase transitions become smoother but occur earlier, and in the higher-frequency range, the phase is negative – meaning that the response to rapid excitations becomes slower.

From a control perspective, at high speed with additional load, there is a higher risk of degraded handling and stability (greater delays and smaller phase margins), which requires more delicate steering inputs or alternative controller settings (e.g. power steering/ESC adjustments).

The frequency response characteristics (magnitude response in linear and decibel scale, and phase response) of steering input Kk and roll velocity response RV for the unloaded and loaded vehicle (W1 and W2) at different driving speeds are presented in Fig. 8, 9 and 10.

In both vehicle states, the overall shape is similar: a distinct peak appears within the 0.9–1.3 Hz range, followed by a steep decline toward approximately 2.0–2.3 Hz (with even a small "dip" around 2.1–2.2 Hz), and low values beyond that range. At low frequencies (< 0.7 Hz), the response is small, then rapidly increases toward the peak. The higher the speed, the greater the amplitude across the entire low/medium-frequency range; the ordering of the curves is nearly monotonic: 64(63) > 56 > 45(44) > 35(34) > 21 km/h. The peak frequency does not change significantly with speed, but at higher speeds the peak becomes more pronounced and higher (e.g. for 64 km/h in W1: 0.33–0.36; in W2: 0.28–0.31). Above 1.8–2.0 Hz, the influence of speed is minor, with the curves converging.

Loading raises the response level in the low-frequency band for the same speeds, especially at 21–45(44) km/h. At 21 km/h, the difference is very clear (W2 distinctly higher than W1). The peak shifts slightly toward lower frequencies and becomes broader – an effect of greater roll inertia (lower natural frequency of the body-suspension system) under load. Above 1.8 Hz, the influence of mass decreases, with the W1 and W2 curves becoming similar and of low magnitude. Beyond 2 Hz, both speed and loading have little effect, as the system is already effectively damped.

From a suspension tuning perspective, at higher speeds, the loaded vehicle requires stronger damping and/or stiffer roll-control components (stabilizers, compression, rebound damping) to limit the peak around 1 Hz and improve both ride comfort and stability.

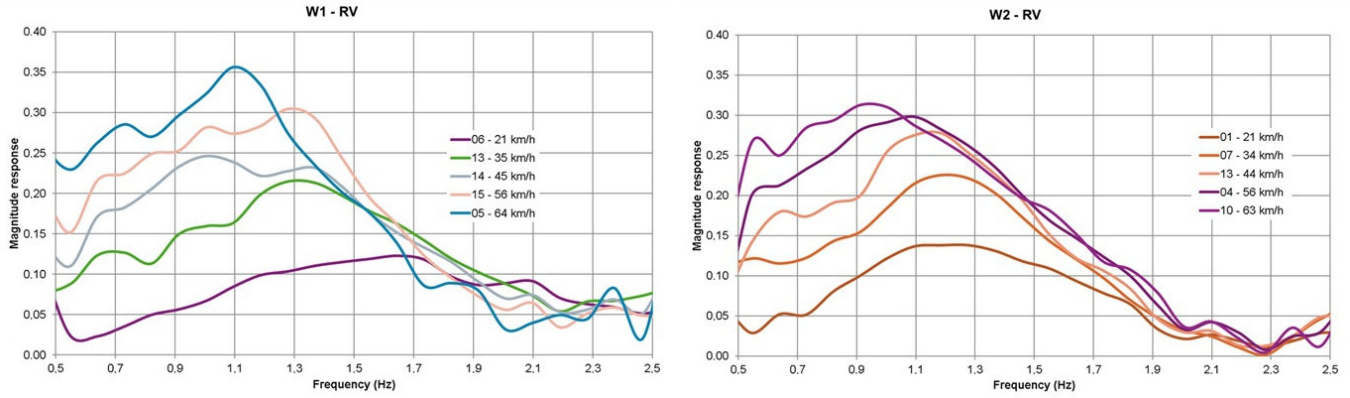

(a) (b)

Fig. 8. Frequency response characteristics (magnitude response) of steering input Kk and roll velocity response RV for the vehicle: (a) unloaded – W1, (b) loaded – W2

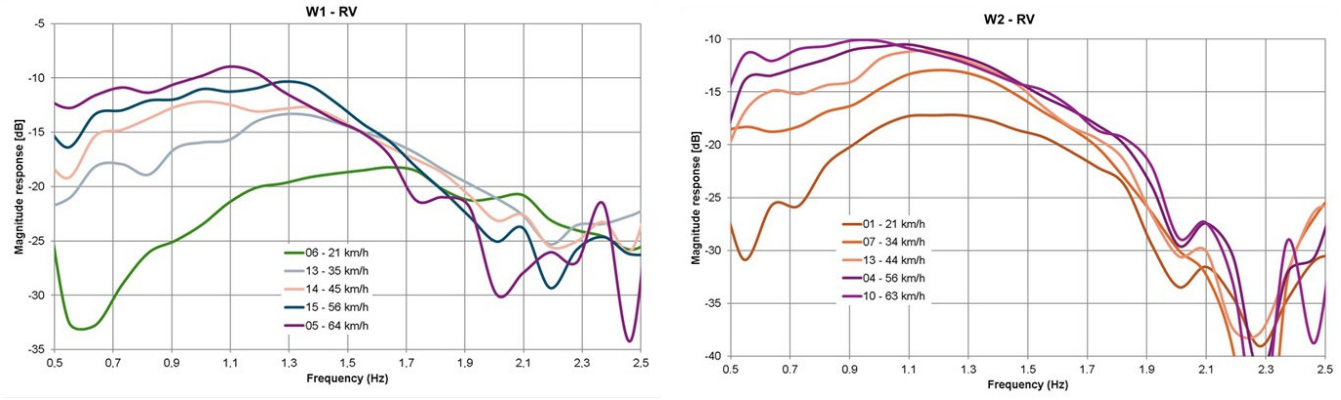

(a) (b)

Fig. 9. Frequency response characteristics (magnitude response on decibel scale) of steering input Kk and roll velocity response RV for the vehicle: (a) unloaded – W1, (b) loaded – W2

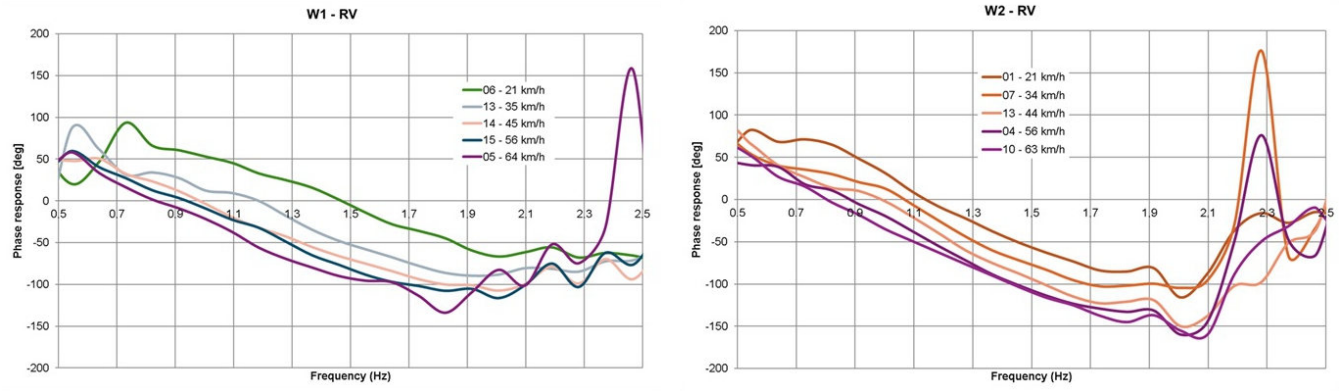

(a) (b)

Fig. 10. Frequency response characteristics (phase response) of steering input Kk and roll velocity response RV for the vehicle: (a) unloaded – W1, (b) loaded – W2

In both states, a peak occurs within the 0.9–1.3 Hz range, followed by a systematic decline up to 2.2–2.4 Hz, with a local dip around 2.1–2.3 Hz. Loading increases the response level (W2 curves are less negative than W1) within the 0.7–1.6 Hz band at comparable speeds, indicating greater roll susceptibility. The peak shifts slightly toward lower frequencies and tends to broaden in the case of W2, which reflects the effect of increased mass and a lower natural frequency of the roll system. Within the 2.1–2.3 Hz range, loading no longer significantly alters the response level, and the W1/W2 differences are minor. Above 2 Hz, both speed and loading have negligible influence, as the system is strongly damped.

In all cases, the phase shifts from positive values (small delay or lead) in the low-frequency range toward strongly negative values (large delay) at medium and higher frequencies. Around 2.3–2.5 Hz, pronounced disturbances occur – local phase jumps (oscillations associated with roll resonances).

The frequency response characteristics (magnitude response in linear and decibel scale, and phase response) of steering input Kk and yaw velocity response YV for the unloaded and loaded vehicle (W1 and W2) at different driving speeds are presented in Fig. 11, 12 and 13.

The curves exhibit a low-pass characteristic: the highest values occur at low frequencies (approx. 0.6–1.2 Hz, forming a gentle hump/plateau), followed by a gradual decline up to 2.4–2.5 Hz. No sharp resonances are observed, and differences between the responses diminish above 2.0 Hz. The loaded vehicle (W2) shows higher magnitude response values across the entire low, medium-frequency range as compared to W1 at the same speeds (greater "yaw gain"). The hump around 0.8–1.1 Hz tends to be slightly higher and broader in W2, reflecting the effect of greater inertia and a lower characteristic frequency. Above 2.0 Hz, the W1–W2 differences disappear, as the system is already strongly damped.

Low-pass behavior is observed: the highest level occurs within the 0.6–1.2 Hz range (a gentle plateau), followed by a decline up to 2.4–2.5 Hz. Above 2.0–2.2 Hz, the curves converge, indicating a reduced influence of operating conditions. Loading increases the response level by approximately 1–3 dB within the 0.6–1.6 Hz band at the same speeds (W2 curves lie higher – less negative). In W2, the maximum around 0.8–1.1 Hz is somewhat more pronounced (broader/higher plateau), which corresponds to a lower characteristic frequency of the system with added mass. Above 2 Hz, the W1–W2 differences are small ($\leq$ 1 dB).

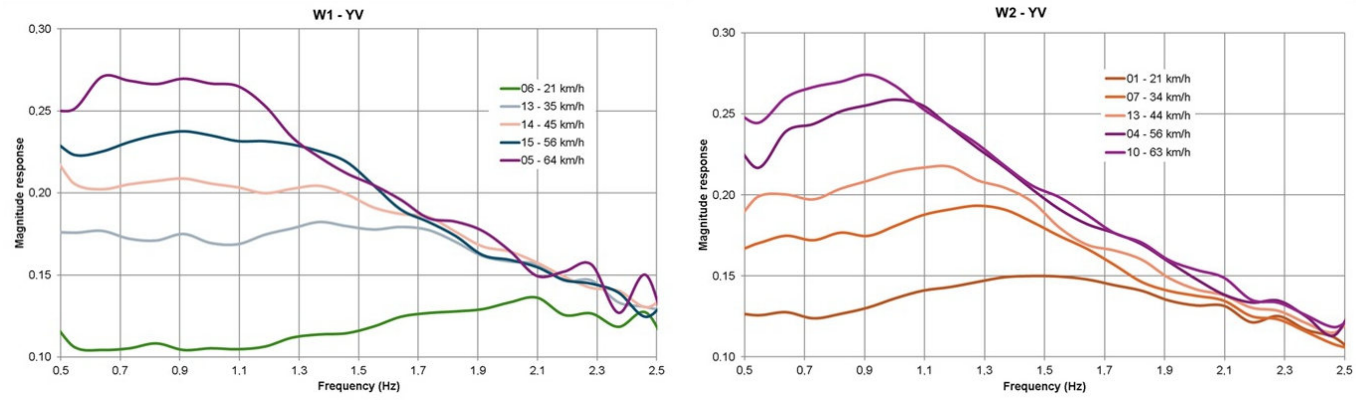

(a) (b)

Fig. 11. Frequency response characteristics (magnitude response) of steering input Kk and yaw velocity response YV for the vehicle: (a) unloaded – W1, (b) loaded – W2

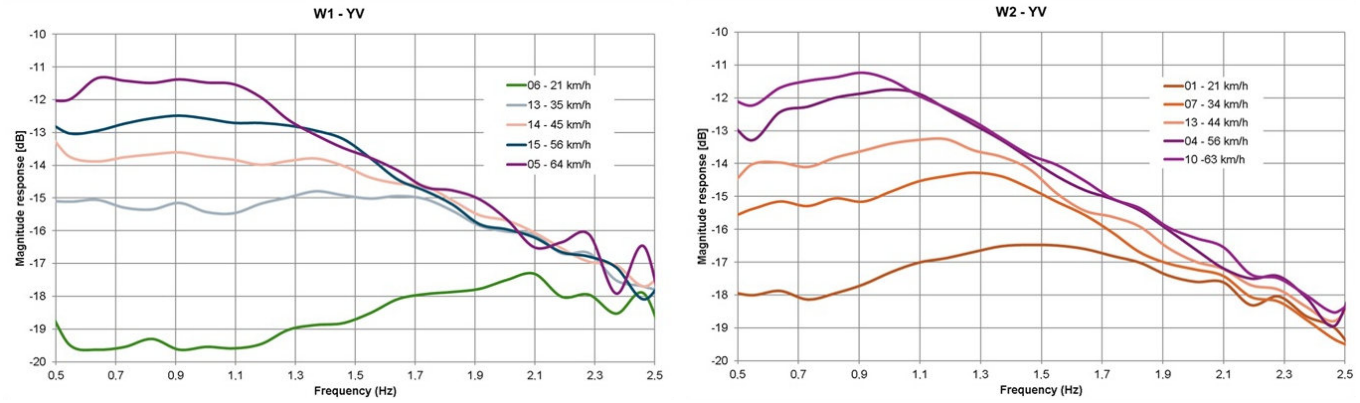

(a) (b)

Fig. 12. Frequency response characteristics (magnitude response on decibel scale) of steering input Kk and yaw velocity response YV for the vehicle: (a) unloaded – W1, (b) loaded – W2

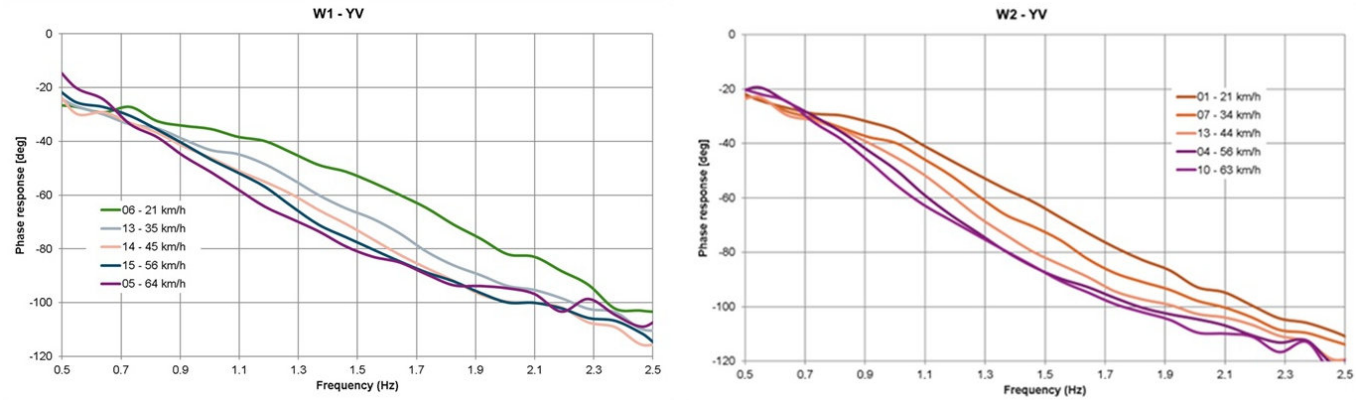

(a) (b)

Fig. 13. Frequency response characteristics (phase response) of steering input Kk and yaw velocity response YV for the vehicle: (a) unloaded – W1, (b) loaded – W2

For all conditions, the phase decreases smoothly from approximately −15/−20° (0.5–0.7 Hz) to about −120° at 2.4–2.5 Hz, i.e. as frequency increases, the yaw velocity response exhibits greater delay relative to steering input. Loading increases the delay: for the same speeds, the W2 curves lie lower (more negative phase), particularly within the 1–2 Hz range. W2 also shows more consistent curves (smaller spread across speeds) and a slightly earlier phase drop with frequency, reflecting the effect

of greater inertia. Around 2.3–2.5 Hz, all curves converge toward −115°, indicating that the influence of speed and mass diminishes.

4.3. Summary of frequency-domain analysis

The observed trends are of a general character and arise from the fundamental principles governing the dynamics of mechanical systems. An increase in vehicle mass results in a reduction of natural frequencies and alters the balance between inertial effects and the elastic and damping forces of the suspension system. These effects occur independently of the specific vehicle type, provided that the underlying mass-spring-damper structure remains comparable. Accordingly, similar modifications in the frequency characteristics of roll rate and lateral velocity can be expected across a wide range of road vehicles, including both passenger cars and commercial vehicles. While the magnitude of these effects depends on factors such as suspension geometry, CG and anti-roll bar stiffness, the qualitative behavior of the system remains consistent.

Changing the configuration from W1 to W2 results in an increase in the magnitude response within the 0.5–2.5 Hz frequency range for all analyzed vehicle speeds. Even at a low speed (21 km/h), configuration W2 exhibits higher magnitude response levels, indicating greater sensitivity of the system to low-frequency, quasi-static excitation as compared to configuration W1.

As the vehicle speed increases, the differences between the two configurations remain and become more pronounced. At 56 km/h, the transition from W1 to W2 leads to a further increase in vibration levels within the analyzed frequency band, accompanied by a shift of the response peak towards lower frequencies, which may result in more perceptible rocking or global structural deflections.

Analysis of lateral velocity shows a clear increase with speed, which means that in the loaded state (W2), the levels are higher than in the unloaded state (W1), particularly within the 0.5–1.5 Hz range. The phase angle for W2 exhibits more negative shifts (greater delay) and earlier transitions. Analysis of roll velocity provides the most distinct difference between W2 and W1 within the 0.9–1.3 Hz frequency range. In W2, the amplitude is higher and slightly shifted toward lower frequencies, reflecting the effect of added mass. Above 2 Hz, the system is strongly damped, and the differences disappear. Analysis of yaw velocity in the W2 variant shows that the levels are 1–3 dB higher within the 0.6–1.6 Hz range, though the difference between W2 and W1 is smaller than for RV. The phase in W2 is more negative, indicating greater delay within the 1–2 Hz range. Among the responses, RV analysis provides the clearest and most repeatable amplitude differences between W2 and W1, with the peak frequency shifted to lower values in W2. These differences appear distinctly already at medium speeds, rather than only at the highest speeds. LV analysis can serve as a supporting channel, since visible differences are present. YV analysis is also useful, though less sensitive (smaller dB increments), and should be treated as supplementary.

In the frequency domain, the following should be compared: the RV peak value and its frequency (W2: higher peak, slightly lower frequency), LV level in 0.5–1.5 Hz (W2 higher), and YV level in 0.6–1.6 Hz (W2 higher by 1–3 dB).

Conclusion: to effectively detect the vehicle load state, tests should be carried out at 45–56 km/h with sinusoidal steering excitation at 1.0 Hz (or within 0.9–1.3 Hz). The primary diagnostic feature is RV (amplitude + peak frequency), supported by LV level and, if necessary, YV. This combination of conditions and response variables provides the highest resolution between W1 and W2 and is practical for on-road implementation.

The proposed method can be implemented using only the RV (roll velocity) signal, which exhibits the highest sensitivity to changes in the vehicle load state. The LV and YV variables are not required for load detection itself; instead, they serve as auxiliary signals that allow verification of the test validity and improve the robustness of the method against disturbances and variability in measurement conditions. Excluding LV and YV does not reduce sensitivity of the RV-based indicator, but it may decrease the confidence of the decision in borderline cases when data quality is degraded.

5. MASS IDENTIFICATION PROCEDURE

A simplified model that accounts for body roll was employed. The model assumes that the vehicle body rolls on a compliant suspension, while the unsprung mass (wheels, axles) is neglected. In the model calculations, a linear second-order oscillator (1-DoF) in roll is used. The input is a sinusoidal steering angle signal δ (Kk), and the output is the roll rate RV, fitted in the vicinity of the resonance at 1 Hz. The entire identification is based solely on the RV channel, RV = $\dot{\varphi}$, excited by a sinusoidal steering input around 1 Hz. The RV data were taken directly from the plots presented above.

The equation of motion for the body roll at small angles has the following form:

$$J_\varphi \ddot{\varphi} + c_\varphi \dot{\varphi} + k_{\text{eff}} \varphi = m_s h a_y , \tag{7}$$

where: J_φ – roll moment of inertia, [kg·m^2]; c_φ – equivalent roll damping, [N·m·s/rad]; m_s – sprung mass, [kg]; h – distance CG from the roll axis, [m]; a_y – vehicle lateral acceleration;

$$k_{\text{eff}} = \left(k_\varphi + m_s g h\right), \tag{8}$$

where: k_φ – roll stiffness coefficient (springs, anti-roll bars, frame and vehicle structure), [N·m/rad].

The presented procedure shows that, by using the measured lateral acceleration a_y and roll response RV, it is possible to determine the roll frequency characteristics and, on this basis, quantitatively estimate the sprung mass of the vehicle. The shift in the resonance frequency between the unloaded and loaded states provides a direct and measurable basis for mass identification. The transfer function (roll 1-DoF) is obtained from the following formula:

$$\left|H_{\varphi\delta}(\mathrm{j}\omega)\right| = \frac{\mathrm{j}\omega K_\delta}{k_\varphi + \mathrm{j}\omega c_\varphi - \omega^2 I_{\text{eff}}} , \tag{9}$$

where: I_{eff} – effective roll moment of inertia (body and payload); K_δ – input parameter that converts the steering command into the roll-exciting moment, estimated jointly with I_{eff}, k_φ, c_φ.

For successive excitation frequencies, the steady-state amplitude of RV was selected. This yielded the RV magnitude response curve as a function of frequency f [Hz]. In the narrow band around the peak, the input amplitude δ(Kk) was assumed to be approximately constant with respect to f. Under this assumption, the shape of the RV peak represents the shape of the transfer function magnitude, and the half-power method can be applied.

The half-power level was determined from the following formula:

$$|H|_{1/2} = |H|_{\max}/\sqrt{2}. \tag{10}$$

A full computation step was selected for the analyzed driving speeds. For each set of RV(f) curves, the peak magnitude $|H|_{\max}$ was identified within the 0.6–1.6 Hz band (peak frequency f_p is given for reference), with particular emphasis placed on the 0.9–1.3 Hz range (the resonance region). Frequencies above 2 Hz were neglected due to strong damping and lack of diagnostic relevance. The half-power frequencies f_1 (left) and f_2 (right) were obtained by linear interpolation. The modal parameters were then determined from the following formulas:

– half-power natural frequency:

$$f_n \approx \sqrt{f_1 f_2}; \tag{11}$$

– natural angular frequency:

$$\omega_n \approx 2\pi f_n. \tag{12}$$

The identified modal parameters for configurations W1 and W2 are summarized in Tables 5 and 6.

Additional assumed constants (calibration values) include $h_{\text{eq}} = 0.3$ m, and sprung mass in the reference condition: $m_s(\text{W1}) = 1840$kg. The 1-DoF roll model (second-order oscillator) is governed by:

$$\omega_n^2 = \frac{k_\varphi}{I_{\text{eff}}}. \tag{13}$$

A geometric approximation is used:

$$I_{\text{eff}} \approx m_s h_{\text{eq}}^2, \tag{14}$$

$$m_s \approx \frac{k_\varphi}{h_{\text{eq}}^2 \omega_n^2}. \tag{15}$$

Since k_φ is not known *a priori*, the reference inertia $I_{\text{eff},1}$ is first determined:

$$I_{\text{eff},1} = m_s(\text{W1}) h_{\text{eq}}^2. \tag{16}$$

From the W1 results, the corresponding roll stiffness is obtained:

$$k_{\varphi,1}(v) = I_{\text{eff},1} \omega_{n,1}(v)^2. \tag{17}$$

It is assumed that the roll stiffness does not change between W1 and W2, i.e.:

$$k_{\varphi,2}(v) \approx k_{\varphi,1}(v). \tag{18}$$

Then the sprung mass for W2 is estimated as:

$$m_s(\text{W2})_{\text{est}}(v) = \frac{k_{\varphi,1}(v)}{h_{\text{eq}}^2 \omega_{n,2}(v)^2}. \tag{19}$$

Table 7 summarizes the input data and calculation results for each W1/W2 speed pair, including the half-power natural frequencies f_n, the identified $k_{\varphi,1}(v)$ from W1 calibration, and the resulting estimated sprung mass $m_s(\text{W2}_{\text{est}}$.

Table 5
Identified modal parameters for configuration W1

Speed [km/h]	f_p [Hz]	$\|H\|_{\max}$	$\|H\|_{1/2}$	f_1 [Hz]	f_2 [Hz]	f_n [Hz]
21	1.642336	0.122687	0.086753	1.109714	1.914013	1.457398
35	1.277372	0.215003	0.15203	0.931577	1.690181	1.254805
45	1.00365	0.246168	0.174067	0.662034	1.557943	1.015584
56	1.277372	0.30471	0.215462	0.63775	1.512466	0.982128
64	1.094891	0.356589	0.252147	0.60898	1.329272	0.899722

Table 6
Identified modal parameters for configuration W2

Speed [km/h]	f_p [Hz]	$\|H\|_{\max}$	$\|H\|_{1/2}$	f_1 [Hz]	f_2 [Hz]	f_n [Hz]
21	1.277372	0.13802	0.097595	0.900228	1.617066	1.206536
34	1.186131	0.225327	0.15933	0.92667	1.50081	1.179303
44	1.186131	0.277629	0.196313	0.87267	1.453106	1.126091
56	1.094891	0.298386	0.21099	0.62261	1.431879	0.944194
63	0.912409	0.312726	0.221131	0.511947	1.36718	0.836614

Table 7
Summary of input data and calculation results for each W1/W2 speed pair

Speed W1/W2 [km/h]	$f_{n,\mathrm{W1}}$ [Hz]	$f_{n,\mathrm{W2}}$ [Hz]	$k_{\varphi,1}$ [N·m/rad]	$m_s(\mathrm{W2})_{\mathrm{est}}$ [kg]
21/21	1.457398	1.206536	13886	2685
35/34	1.254805	1.179303	10294	2083
45/44	1.015584	1.126091	6743	1497
56/56	0.982128	0.944194	6306	1991
64/63	0.899722	0.836614	5292	2128

The estimates for speed pairs 35/34, 56/56 and 64/63 km/h are consistent (approximately 1991–2128 kg). The estimates for 21/21 km/h are overestimated, while those for 45/44 km/h are underestimated; thus, the parameters appear to depend on speed, while other effects (lateral-yaw coupling, nonlinearities, amplitude effects, etc.) become mixed in. According to the diagnostic recommendation for the driving speed range of 45–56 km/h and those yielding stable identification within this data set, the 45/44 point is treated as an outlier, and stabilization is performed using 35/34, 56/56 and 64/63. The arithmetic mean is 2067 kg, while the median is 2083 kg. The spread in this set, expressed as standard deviation, is approximately 70 kg – reference value (2060 kg).

The presented procedure shows that, using 1-DoF, it is possible to determine the roll frequency characteristics and, on this basis, quantitatively estimate the vehicle mass, but the use of the 1-DoF model may lead to a large scatter of calculation results.

6. SUMMARY

In contrast to previous studies that primarily focus on vehicle mass estimation using complex algorithms or high-frequency acceleration signals, this work adopts a simplified dynamic representation based on a 1-DoF oscillator. The proposed approach defines practical road-test conditions, including an appropriate vehicle speed range and excitation frequency band, under which the system response is dominated by a single dynamic mode. The application of a linear 1-DoF oscillator model enables an effective correlation between changes in the vehicle's dynamic response parameters and its total mass. Owing to its simplicity and clear physical interpretation of dynamic parameters, the model can be successfully used for fast and computationally efficient identification of the vehicle load condition. The results obtained confirm that even a simplified representation of vehicle dynamics is sufficient to capture the key relationships between mass and system response. However, certain limitations of this approach should be noted, primarily resulting from the linear nature of the model and the reduction of real vehicle dynamics to a single degree of freedom. The model does not account for suspension nonlinearities, variations in damping characteristics, or coupling between different body motions, which may reduce its accuracy under conditions of large excitation amplitudes, high driving speeds or varying road surface properties. In such cases, the use of higher-order models or adaptive identification methods may be required.

REFERENCES

[1] M. Nowakowski and J. Kuryło, "Usability of perception sensors to determine the obstacles of unmanned ground vehicles operating in off-road environments," *Appl. Sci.*, vol. 13, no. 8, p. 4892, 2023, doi: 10.3390/app13084892.

[2] L. Prochowski, P. Szwajkowski, and M. Ziubiński, "Research scenarios of autonomous vehicles, the sensors and measurement systems used in experiments," *Sensors*, vol. 22, p. 6586, 2022, doi: 10.3390/s22176586.

[3] M. Guzek, "Car ADR/EDR recorders – uncertainty of vehicle's speed and trajectory determination," *Arch. Transp.*, vol. 22, no. 2, pp. 163–174, 2010, doi: 10.2478/v10174-010-0010-5.

[4] T. Pusty *et al.*, "Research on the possibility of carrying out convoy driving missions using vehicles with varying degrees of autonomy," *Arch. Transp.*, vol. 72, no. 4, pp. 7–21, 2024, doi: 10.61089/aot2024.xdtvm09.

[5] R.S. Jurecki, T.L. Stańczyk, and M. Ziubiński, "Analysis of the structure of driver maneuvers in different road conditions," *Energies*, vol. 15, p. 7073, 2022, doi: 10.3390/en15197073.

[6] A. Dębowski, J.J. Faryński, and D.P. Żardecki, "Reference models of 4WS vehicle lateral dynamics for the synthesis of steering algorithms," in *Perspectives in Dynamical Systems II – Numerical and Analytical Approaches (DSTA 2021)*, J. Awrejcewicz, Ed., *Springer Proceedings in Mathematics & Statistics*, vol. 454, Cham: Springer, 2024, doi: 10.1007/978-3-031-56496-3_11.

[7] J. Faryński, D. Żardecki, and A. Dębowski, "Method of autonomous vehicle control using simplified reference models and regulators," *Probl. Mechatron. Armament Aviat. Saf. Eng.*, vol. 14, no. 4, pp. 37–58, 2023, doi: 10.5604/01.3001.0054.164.

[8] T. Pusty, Determining the trajectory of the vehicle motion on the basis of the recorded physical quantities describing its dynamics during double lane change maneuvers," *Arch. Automot. Eng. – Arch. Motoryz.*, vol. 96, no. 2, pp. 96–102, 2022, doi: 10.14669/AM/151703.

[9] L. Prochowski *et al.*, "Impact of control system model parameters on the obstacle avoidance by an autonomous car–trailer unit: research results," *Energies*, vol. 14, p. 2958, 2021, doi: 10.3390/en14102958.

[10] P. Lugner and M. Plöchl, "Modelling in vehicle dynamics of automobiles," *ZAMM-Z. Angew. Math. Mech. (J. Appl. Math. Mech.*, vol. 84, no. 4, pp. 219–236, 2004, doi: 10.1002/zamm.200310108.

[11] M. Plöchl and J. Edelmann, "Driver models in automobile dynamics application," *Veh. Syst. Dyn.*, vol. 45, no. 7–8, pp. 699–741, 2007, doi: 10.1080/00423110701432482.

[12] T. Pusty, P. Simiński, J. Jackowski, E. Kostecka, and L. Chybowski, "Dynamic load on the head during rear impact against a headrest," *Adv. Sci. Technol. Res. J.*, vol. 19, no. 7, pp. 313–327, 2025, doi: 10.12913/22998624/203858.

[13] R. Lopes, B.V. Farahani, F. Queirós de Melo, and P.M.G.P. Moreira, "A dynamic response analysis of vehicle suspension system," *Appl. Sci.*, vol. 13, no. 4, p. 2127, 2023, doi: 10.3390/app13042127.

[14] W. Pieniążek, S. Walczak, and G. Motrycz, "Study of the Response of a Four-Axle Vehicle to Random Excitation Induced by Steering Wheel Rotation," *Technical Transactions. Mechanics*, Cracow University of Technology Press, no. 8, 3-M/2012.

[15] T. Pusty, P. Simiński, W. Kupicz, and M. Mieteń, "Dynamic characteristics of vehicle steerability as a tool for assessing vehicle dynamic properties and technical condition," in *Challenges of Technical Security for Newly Introduced Equipment in the Armed Forces*, Radom: Scientific and Publishing Institute "Spatium," 2024.

[16] W. Luty and T. Pusty, "Analysis of dynamic characteristics of vehicle steerability in the context of its diagnostics and evaluation of dynamic properties," in *Proc. 16th Int. Conf. Dynamical Systems Theory and Applications (DSTA)*, Dec. 6–9, 2021. [Online]. Available: https://cybra.lodz.pl/dlibra/publication/23715/edition/20465/content

[17] F. Mancosu and C. Savi, "Vehicle sensitivity to tyre characteristics both in open and closed loop manoeuvres," presented at the *2000 European Adams Conference*, Rome, Italy, November 15–16, 2000.

[18] W. Chu, K. Cao, S. Li, Y. Luo, and K. Li, "Vehicle mass estimation based on high-frequency information extraction," in *Proc. 7th IFAC Symposium on Advances in Automotive Control*, Tokyo, Japan, September 4–7, 2013, doi: 10.3182/20130904-4-JP-2042.00022.

[19] T. Vu, "Annals of DAAAM for 2012 & Proceedings of the 23rd International DAAAM Symposium," *DAAAM International*, Vienna, Austria, 2012.

[20] D. Joshi, S. Kedia, and S. Muthiah, "A study on the effect of steering input frequency on transient lateral dynamics of four-wheeled passenger vehicles," *SAE Tech. Pap.*, 2019-26-0070, 2019, doi: 10.4271/2019-26-0070.

[21] M. Sultan, G. Heydinger, N. Durisek, and D. Guenther, "A study of vehicle class segregation using linear handling models," *SAE Tech. Pap.*, 950307, 1995, doi: 10.4271/950307.

[22] Z. Wang, J. Zhong, J. Hu, Z. Zhang, and W. Zhao, "Mass estimation-based path tracking control for autonomous commercial vehicles," *Appl. Sci.*, vol. 15, no. 2, p. 953, 2025, doi: 10.3390/app15020953.

[23] G. Liu, "Estimation of vehicle mass and road slope for commercial vehicles utilizing an interacting multiple-model filter method under complex road conditions," *World Electr. Veh. J.*, vol. 16, p. 172, 2025, doi: 10.3390/wevj16030172.

[24] B. Feng, G. Yin, Y.en, T. Shen, and F.A Wang, "Joint Vehicle Mass and Road Slope Estimation of Distributed Drive Electric Vehicles Considering Road Environment Factors," in *Proc. International Conference on Intelligent Transportation Systems (ITSC)*, Macau, China, 8–12 October 2022; pp. 817–824.